Journal of Nuclear Medicine, published on December 18, 2014 as doi:10.2967/jnumed.114.148106

Whole-body PET/CT Evaluation of Tumor Perfusion using Generator-based ^{62}Cu-ETS: Validation by Direct Comparison to ^{15}O-Water in Metastatic Renal Cell Carcinoma

James W. Fletcher,[a] Theodore F. Logan,[b] Jacob A. Eitel,[a] Carla J. Mathias,[a] Yen Ng,[a] Jeffrey L. Lacy,[c] Gary D. Hutchins,[a] and Mark A. Green[a]

[a]Department of Radiology and Imaging Sciences, Indiana University School of Medicine, Indianapolis, IN, the [b]Melvin & Bren Simon Cancer Center, Indiana University School of Medicine, Indianapolis, IN, and [c]Proportional Technologies, Inc., Houston, TX

First and corresponding author: James W. Fletcher, M.D.
Department of Radiology and Imaging Sciences
Indiana University School of Medicine
550 North University Avenue Room, 0655A
Indianapolis, IN 46202
317-944-1800
jwfletch@iupui.edu

Supported by grants from the Melvin and Bren Simon Cancer Center and the National Cancer Institute of the National Institutes of Health (R01-CA140299).

Running title: *^{62}Cu-ETS PET Tumor Perfusion Imaging*

Abstract

This study was undertaken to: *(i)* demonstrate the feasibility of whole-body ^{62}Cu-ETS PET/CT tumor perfusion imaging in patients with metastatic renal carcinoma; and *(ii)* validate ^{62}Cu-ETS as a quantitative marker of tumor perfusion by direct comparison with ^{15}O-water perfusion imaging. **Methods.** PET/CT imaging of 10 subjects with stage IV renal cell cancer was performed after i.v. administration of ^{15}O-water (10-minute dynamic list mode study) with the heart and at least one tumor in the PET field-of-view, followed 10-minutes later by i.v. ^{62}Cu-ETS (6-minute list mode study). Whole body ^{62}Cu imaging was then carried out from 6-20 minutes at 2-3 minutes/bed. Blood flow (K_1) was quantified with both agents for normal and malignant tissues in the 21.7 cm dynamic field-of-view. The required arterial input functions were derived from the left atrium, and in the case of ^{62}Cu-ETS, corrected for partial decomposition of the agent by blood using data from an *in vitro* analysis using a sample of each patient's blood. This imaging protocol was repeated at an interval of 3-4 weeks following initiation of a standard clinical treatment course of the anti-angiogenic agent sunitinib. **Results.** All subjects received the scheduled ^{62}Cu-ETS doses for the dynamic and subsequent whole-body PET/CT scans, but technical issues resulted in no baseline ^{15}O-water data for two subjects. Direct comparisons of the perfusion estimates for normal tissues and tumor metastases were made in 18 paired baseline and treatment studies (10 subjects; 8 baseline studies, 10 repeat studies during treatment). There was an excellent correlation between the blood flow estimates made with ^{62}Cu-ETS and ^{15}O-water for normal tissues (muscle, thyroid, myocardium) and malignant lesions (pulmonary nodules, bone lesions); the regression line was $y = 0.85x + 0.15$, $R^2 = 0.83$, for the 88 regions analyzed. **Conclusions.** ^{62}Cu-ETS provided high quality whole-body PET/CT images, and ^{62}Cu-ETS measures of blood flow were highly and linearly correlated with ^{15}O-water derived K_1 values ($mL^{-1} \cdot min^{-1} \cdot g$). This tracer is suitable for use as a PET tracer of tumor perfusion in patients with metastatic renal cell carcinoma.

Key Words: Tumor perfusion

Copper-62 PET

^{62}Cu-ETS [ethylglyoxal bis(thiosemicarbazonato)copper(II)]

^{15}O-water

Renal cell carcinoma

Introduction

The clinical care of cancer patients often demands diagnostic methods that are suitable for whole body imaging, due to varied and distributed nature of metastatic disease. Thus, whole-body scanning is a clinical standard in metabolic imaging of tumors with ^{18}F-FDG, as well as in imaging to detect skeletal metastases based on rates of bone remodeling, and in the imaging of neuroendocrine tumors using somatostatin-receptor-targeted agents. A technique for whole-body assessment of tumor perfusion would naturally complement metabolic imaging in definition of the tumor microenvironment, and could also assist in evaluation of patient response to antiangiogenic therapies.

Rationale for measuring tumor perfusion. The growth rates of solid tumors are often limited by their capacity to recruit vasculature for nutritive perfusion (*1-3*), leading to widespread interest in tumor vascular endothelium as a target for the action of chemotherapeutic drugs (*4,5,6*). Tumor vasculature is morphologically abnormal (*2,7*), and unlike normal tissues, the rates of tumor perfusion and metabolism are often uncoupled and unpredictably heterogeneous. The heterogeneity of tumor perfusion impacts the efficiency of drug delivery, while also leading to zones of hypoxia that may be quite resistant to treatment by radiation therapy (*8-10*). A whole-body scanning technique for assessment of tumor perfusion would potentially complement standard whole-body ^{18}F-FDG imaging of tumor metabolism, offering further insights into the physiology of a patient's tumors and their response to treatment (*10*).

^{15}O-water tumor perfusion measurements. Oxygen-15-labeled water is the "gold standard" for PET quantification of regional tissue perfusion, having been validated to behave as a freely-diffusible tracer in myocardium (*11-14*), and to also robustly allow quantification of cerebral blood flow (*15,16*). As a freely diffusible tracer, ^{15}O-water is also the standard for non-invasive

imaging to quantify tumor perfusion (*17-20*). The 2-minute physical half-life of ^{15}O is ideally suited to imaging at high activity levels over the intrinsically brief time interval in which the distribution of a freely diffusible tracer is dominated by its perfusion-rate-limited delivery to tissue. However, for routine clinical imaging of tumor perfusion, ^{15}O-water faces significant technical and practical barriers, including: *(i)* the need for an on-site cyclotron for ^{15}O production; *(ii)* the intrinsic need to image ^{15}O-water at very high count rates in order to obtain good counting statistics; *(iii)* imaging being constrained to a single position of the scanner bed, precluding flow assessment using whole-body imaging protocols of the type routinely employed in clinical oncology studies with ^{18}F-FDG; and *(iv)* the need for invasive arterial blood sampling following each ^{15}O-water injection, if flow is to be quantified and the heart, or another large arterial blood pool region, falls outside the camera's field-of-view.

The ^{62}Cu-generator and copper(II) bis(thiosemicarbazone) perfusion tracers. The $^{62}Zn/^{62}Cu$ generator system has the potential to provide widespread routine clinical access to short-lived ^{62}Cu (9.7-minute half-life) for PET/CT imaging without the limitations of oxygen-15 (*21-23*). Copper(II) bis(thiosemicarbazone) complexes, most notably Cu-PTSM [pyruvaldehyde *bis*(N^4-methylthiosemicarbazonato)copper(II)] and Cu-ETS [ethylglyoxal *bis*(thiosemicarbazonato)copper(II)], have shown promise for use as ^{62}Cu-radiopharmaceuticals for perfusion imaging with PET (*21*,*22*,*24-33*). In addition to exhibiting the desired high first-pass tissue extraction of tracer, these agents also desirably afford prolonged "microsphere-like" tissue retention of the radiolabel (*24*,*33-35*), as they undergo rapid intracellular reductive decomposition liberating ionic ^{62}Cu into the endogenous intracellular copper pool (*36-37*). For human studies, ^{62}Cu-ETS should be superior to ^{62}Cu-PTSM for perfusion assessment in high-flow tissues, because it avoids Cu-PTSM's strong species-specific association with human serum albumin (*38*,*39*).

Objectives of this study. The purpose of the present study was: *(i)* to demonstrate the feasibility of whole-body ^{62}Cu-ETS PET/CT tumor perfusion imaging in patients with metastatic renal carcinoma; and *(ii)* to begin validation of ^{62}Cu-ETS as a quantitative marker of tumor perfusion by direct comparison to ^{15}O-water perfusion imaging.

Methods and Materials:

The study protocol was approved by the Indiana University institutional review board. All patients had a diagnosis of advanced Stage IV renal cell cancer (RCC) and agreed to participate in the study following informed consent. The primary renal cell cancer had been surgically removed in all of our subjects.

Radiopharmaceuticals.

Proportional Technologies, Inc. (Houston, TX) produced the required ^{62}Zn/^{62}Cu-generators, as well as the lyophilized cold kits and reagents for on-demand preparation of the ^{62}Cu-ETS radiopharmaceutical. Details of generator and radiopharmaceutical kit performance are reported elsewhere (*23*). Patient imaging with ^{62}Cu-ETS was performed under IND #75,018 held by Proportional Technologies, Inc. ^{15}O-water was prepared to the specifications of its USP monograph by the PET Radiochemistry Core of the Indiana Institute for Biomedical Imaging Sciences.

Imaging Protocols and Procedures.

All imaging studies were performed on a 64-slice Siemens True-D Biograph PET/CT. Following a CT exam for attenuation correction in a single bed position centered over the thorax (with the field-of-view including at least one known tumor site, as well as the heart for image-based reconstruction of the ^{15}O-water arterial blood time-activity curve), a 10-minute dynamic list-mode acquisition was carried out upon intravenous administration of ^{15}O-water (20.7 ± 3.2 mCi; 0.766 ± 0.118 GBq; n = 18). This was followed by a 10-minute delay to allow for decay of the ^{15}O. A dynamic list-mode acquisition was then carried out for 6 minutes in the same bed position after intravenous administration of ^{62}Cu-ETS (17.2 ± 3.5 mCi; 0.64 ± 0.13 GBq; n = 20.) An additional CT exam of the whole body was then performed to provide attenuation correction for

the whole body PET/CT ^{62}Cu-ETS exam. Whole-body ^{62}Cu images were then acquired from 6-20 minutes post ^{62}Cu-ETS injection (2-3 minutes per 21.6 cm bed position), allowing assessment of the perfusion distribution in normal tissue and tumor sites outside the initial, single-bed field-of-view. This imaging protocol was repeated following initiation of a standard 3-4 week clinical treatment course of sunitinib.

In Vitro Assay to Define the Kinetics of ^{62}Cu-ETS Decomposition by Patient Blood.

Because a portion of the injected ^{62}Cu-ETS radiopharmaceutical will be reductively decomposed by the patient's blood cells, *in vitro* assays were performed to directly examine the rate of ^{62}Cu-ETS decomposition by patient blood, allowing correction of the PET-derived arterial blood ^{62}Cu time-activity curve to represent the fraction of blood radioactivity expected to remain present as intact ^{62}Cu-ETS (*27,33,40*). Details of this method are presented in the on-line Supplemental Data.

PET/CT Data Analysis.

Three-dimensional volumes of interest were generated using the MIM software *PET Edge* tool (MIM Software, Inc., Cleveland, Ohio) for normal tissues (muscle, thyroid, myocardium, ventricular blood pools) and any malignant lesions that were identified in the 21.7 cm field of view used for dynamic list mode acquisition. The standard two-compartment model routinely employed for the measurement of blood flow in the brain and heart was applied to the measurement of tumor perfusion with ^{15}O-water (*11-17*). Details are presented in the accompanying on-line Supplemental Data. Briefly, in this model the transport of the tracer from the vasculature to the interstitial space is assumed to be sufficiently rapid that the single-pass extraction fraction of water is approximately equal to 1.0 across the range of perfusion values. This model consists of two rate constants, K_1 and k_2, representing the tissue perfusion and tracer washout rates, respectively. Both model rate constants are related to tissue perfusion with:

$$K_1 = \text{RBF x EF } k_2 = \text{RBF} / V_d.$$

In these equations *RBF* is regional blood flow, *EF* is the tracer single-pass extraction fraction, and V_d is the tracer volume of distribution in tissue. For the lung metastases, if the dynamic data showed radiotracer arriving at tumor prior to arrival in the left ventricular blood pool, the radionuclide in the right ventricular blood volume was used to define that lesion's arterial input function. For all other tissues, modeling for flow quantification was based on an input function derived from an ROI for the blood pool of the left ventricle or atrium.

For ^{62}Cu-ETS PET, flow was quantified using a 2-compartment model that was previously used with success in myocardial flow quantification with ^{62}Cu-PTSM (*27,29*). The model was fit using an image-derived input function, analogous to the ^{15}O-water study, corrected to account for partial ^{62}Cu-ETS decomposition in the blood (*27,33,40*).

In addition to the modeling to obtain quantitative tumor perfusion measurements from the dynamic ^{62}Cu-ETS data, we also quantified normal tissue and tumor uptake of ^{62}Cu-ETS as standardized uptake values (SUV) using the attenuation-corrected whole-body exam and 3-D volumes of interest (VOI). SUV values were obtained for normal tissues (muscle, thyroid, myocardium, right ventricular blood pool, lung, left atrial blood pool, liver, pancreas and kidney), as well as for any areas of increased tracer localization representing metastatic RCC in the lungs or bone. Mean and Maximum SUV measurements were obtained and normalized to body weight SUV_{bw} and lean body mass SUV_{lbm}.

Results

The study enrolled 10 subjects, 2 female and 8 male. Average age was 62.8 ± 8.5 years (range 49-77), and body mass 86.4 ± 21 kg (range 60.7-113.5 kg). All subjects had diagnosis of advanced stage renal cell cancer with metastatic skeletal and/or metastatic pulmonary nodular disease. The average time interval between the baseline and repeat (during sunitinib treatment) PET/CT studies was 32 ± 9 days (range 21-49 days).

Eighteen (18) dynamic ^{15}O-water studies were successfully carried out. (Technical difficulties prevented baseline ^{15}O-water imaging in two subjects.) All 10 subjects received the scheduled pre-treatment and during-treatment doses of ^{62}Cu-ETS for dynamic list-mode imaging, and the subsequent companion whole body PET/CT acquisition. Vital signs were monitored before, during and after administration of the ^{62}Cu-ETS, and no changes were observed. No adverse events were noted.

Examples of images from dynamic list mode acquisitions of the two tracers, and a whole-body ^{62}Cu-ETS acquisition, are shown in Figures 1 and 2. The ^{62}Cu-ETS radiopharmaceutical is rapidly cleared from the blood (Figure 3), but the image-derived arterial input function does need to be corrected for the partial decomposition of tracer by blood cells. This correction was made on a study-by-study basis, using the rate of ^{62}Cu-ETS decomposition measured with a sample of that patient's blood at 37°C *in vitro*. The decomposition of ^{62}Cu-ETS by blood always exhibited first-order kinetics, but the reaction rate was quite variable (half-time of decomposition averaging 115 ± 87 seconds, n = 19, or 96 ± 27 seconds with the omission of a blood sample for which the decomposition rate appeared anomalously slow).

Direct comparison of the ^{15}O-water and ^{62}Cu-ETS perfusion estimates were made for 88 regions from the 18 paired dynamic ^{15}O-^{62}Cu scans, representing normal tissues (myocardium, thyroid, and muscle, n = 18, 17, and 18, respectively), plus a total of 35 metastatic lesions (Figure 4). An excellent linear correlation was observed between the blood flow measurements obtained with ^{62}Cu-ETS and the ^{15}O-water reference standard ($y = 0.85x + 0.15$, $R^2 = 0.83$). The data for the tumors increases the observed variance in this analysis. When restricted to only the data for myocardial, thyroid, and muscle regions-of-interest, the regression line becomes $y = 0.97x + 0.09$, $R^2 = 0.90$, while the tumor data alone are fit by the line $y = 0.70x + 0.27$, $R^2 = 0.72$ (Figure 5).

Table 1 compares the K_1-values of both tracers in normal tissue and for the metastatic lesions. Paired 2-tailed t-test values for all tissues and lesions, with the exception of skeletal muscle (where the flow values are very low), also indicate no significant difference between the ^{15}O-water and ^{62}Cu-ETS measurements of tissue perfusion. The ^{62}Cu-ETS measurements of blood flow ($mL^{-1} \cdot min^{-1} \cdot g$) from dynamic list mode data are also well correlated with whole-body ^{62}Cu-ETS SUV values (Figure 6; $y = 0.20x + 0.06$, $R^2 = 0.73$).

Nine of the patients had pulmonary nodules. Five of these had solitary nodules. The average size (RECIST-long diameter) of the nodules at baseline and during the conclusion of therapy is shown in Table 2. An average decrease in size of 29.4% was noted.

Discussion

The current study provides general validation of ^{62}Cu-ETS as a PET tracer of tumor perfusion in patients with metastatic renal cell carcinoma, with the ^{62}Cu-ETS radiopharmaceutical delivering flow values equivalent to those from the best available reference standard – ^{15}O-water. The model-derived K_1 values from the sequential ^{15}O-water and ^{62}Cu-ETS studies were highly correlated, both by linear regression and paired two-tailed T-test, for the tumors as well as the concurrently imaged myocardium and thyroid (Figure 4, Figure 5, and Table 1). Deviation of the correlation of ^{62}Cu-ETS and ^{15}O-water blood flow measurements from the ideal slope of 1.0 (Figures 4 and 5) is largely driven by the data from the lower flow metastatic lesions in the lungs, perhaps reflecting the need for a more refined approach to ^{62}Cu-ETS modeling in pulmonary lesions (*e.g.,* better correcting for count spill-over into the tumor from the less dense surrounding lung).

Despite the short 9.7-minute half-life of ^{62}Cu, high-quality whole-body images were easily obtained with ^{62}Cu-ETS (Figure 2) following initial imaging with the heart in the field-of-view to define the arterial blood time-activity curve. Blood clearance of ^{62}Cu-ETS was rapid, with virtually no intact radiopharmaceutical remaining in blood at the conclusion of our initial 6-minute dynamic acquisition (Figure 3). We believe further work will allow validation of a modeling approach for conveniently extracting quantitative perfusion values from such whole-body scans. The ability to perform whole-body scans is particularly important in evaluation of patients with known or possible metastatic disease, due to the inherently varied and distributed nature of potential lesion presentation.

Laking and Price (*10*) have presented an excellent review of the current status of physiologic PET and SPECT imaging of perfusion and hypoxia as related to angiogenesis. In brief, they conclude that measurement of perfusion with radionuclides is the best biomarker for angiogenesis, and that PET functional imaging has the potential to reveal much about tumor circulation and the effect of treatment. The most successful results have been seen using ^{15}O-water. But, there will always be substantial technical limitations to widespread implementation of the ^{15}O-water method, including: the requirements for an on-site cyclotron; restriction to a single bed position by the required dynamic imaging; and the need for invasive arterial blood sampling to obtain arterial input function, if the heart and tumor(s) are not in a common field-of-view. In spite of these limitations, ^{15}O-water does remain the reference standard for perfusion measurements in humans.

The reported results indicate that, as a short-lived microsphere-like agent, ^{62}Cu-ETS potentially overcomes the practical limitations of ^{15}O-water for quantitative clinical imaging of perfusion. The centrally manufactured and distributed ^{62}Zn/^{62}Cu generator, and companion kits for rapid on-demand radiopharmaceutical synthesis, can make ^{62}Cu-ETS perfusion imaging available to virtually any clinical PET site in the United States. Additionally, the kinetics of ^{62}Cu-ETS enable whole-body scanning, with high quality images being obtained despite the short radionuclide half-life (Figure 2). Furthermore, the 9.7-minute half-life of ^{62}Cu ideally complements companion imaging with ^{18}F-FDG for assessment of tissue metabolism, since the ^{62}Cu will be essentially completely decayed during a standard FDG uptake period, if the FDG is simply administered at the conclusion of ^{62}Cu-image acquisition.

Whole-body ^{62}Cu-ETS SUV values (Figure 6) may be useful for evaluating relative perfusion within a given subject; however, the assessment of perfusion with ^{62}Cu-ETS will be most robustly modeled using the arterial blood input function as the basis for normalizing tissue

levels of ^{62}Cu in the whole-body images. The use of the SUV calculation to normalize tissue concentrations of radiotracer is expected to be somewhat unsatisfactory when employing a tracer that exhibits essentially perfusion-rate-limited delivery to tissue, since the fractional distribution of cardiac output to major organs should largely be independent of total body mass. While more technically demanding than a simple SUV calculation, the microsphere-like tissue trapping of the ^{62}Cu radiolabel should allow robust, and reasonably convenient, ^{62}Cu-ETS perfusion measurements in the whole-body scans by applying an image-derived arterial input function of the type acquired in the present dynamic studies.

The lung lesions were somewhat demanding in the modeling for flow quantification, due to the need to define whether individual tumors derived their arterial blood flow from the pulmonary, or brachial, artery. This is a problem that will be unique to lung metastases, and differentiation of the perfusion source proved readily feasible by kinetic analysis of the dynamic data acquired for image-based definition of the blood input function based on cardiac ROIs.

Limitations of the present study include the limited total number of subjects, and the focus solely on metastatic renal cell carcinoma. Because of the study design, repeatability was not defined. The ^{62}Cu half-life certainly allows a study design involving replicate imaging to directly assess test-retest reproducibility. But, in consideration of the medical condition of these patient volunteers, that additional data collection was judged to be best deferred to a follow-on study. Expansion of this validation protocol is now underway for assessment of ^{62}Cu-ETS performance in a broader array of tumors.

CONCLUSION

This study demonstrates that ^{62}Cu-ETS can be employed as an alternative to ^{15}O-water for tumor perfusion imaging in patients with metastatic renal cell carcinoma, and illustrates the feasibility of whole-body PET/CT imaging with ^{62}Cu, despite its short half-life, using a radiopharmaceutical that produces tissue trapping of the radionuclide.

ACKNOWLEDGEMENTS

This work was supported by grants from the Melvin and Bren Simon Cancer Center and the National Cancer Institute of the National Institutes of Health (R01-CA140299). The content is solely the responsibility of the authors and does not necessarily represent the official views of the National Institutes of Health.

References

1. Hirst DG. Blood flow and its modulation in malignant tumors. In *Microspheres and Regional Cancer Chemotherapy*, N. Willmott and J.M. Daly, eds., Boca Raton, FL: CRC Press; 1994:31-56.
2. Ruoslahti, E. Specialization of tumor vasculature. *Nat Rev Cancer*. 2002;2:83-90.
3. Plank MJ, Sleeman BD. Tumor-induced angiogenesis: a review. *J Theor Med*. 2003; 5:137-153.
4. Zetter BR. Angiogenesis and tumor metastasis. *Ann Rev Med*. 1998;49:407-424.
5. Molema G. Design of vascular endothelium-specific drug-targeting strategies for the treatment of cancer. A*cta Biochim Polonica*. 2005;52:301-310.
6. Featherstone J, Griffiths S. Drugs that target angiogenesis. *Nat Rev Drug Discovery*. 2002;1:413-414.
7. Gillies RJ, Schornack PA, Secomb YW, Raghunand N. Causes and effects of heterogeneous perfusion in tumors. *Neoplasia*. 1999;1:197-207.
8. Moeller B, Cao Y, Vujaskovic Z, Li C, Haroon Z, Dewhirst M. The relationship between hypoxia and angiogenesis. *Semin Radiat Oncol*. 2004;14:215–221.
9. Eriksen JG, Horsman MR. Tumour hypoxia – a characteristic feature with a complex molecular background, *Radiother Oncol*. 2006;81:119-121.
10. Laking G, Price P. Radionuclide imaging of perfusion and hypoxia. *Eur J Nucl Med Mol Imaging*. 2010;37 Suppl 1:S20-S29.
11. Bergmann SR, Fox KA, Rand AL, et al. Quantification of regional myocardial blood flow in vivo with $H_2{}^{15}O$. *Circulation*. 1984;70:724–733.
12. Huang S-C, Schwaiger M, Carson RE, et al. Quantitative measurement of myocardial blood flow with oxygen-15 water and positron computed tomography: an assessment of potential and problems. *J Nucl Med*. 1985;26:616–625.

13. Herrero P, Markham J, Bergmann SR. Quantitation of myocardial blood-flow with (H2O)-O-15 and positron emission tomography—assessment and error analysis of a mathematical approach. *J Comput Assist Tomogr*. 1989;13:862–873.

14. Hutchins GD, Caraher J, Raylman RR. A region of interest strategy for minimizing resolution distortions in quantitative myocardial PET studies. *J Nucl Med*. 1992;33:1243-1250.

15. Frackowiak RSJ, Lenzi G-L, Jones T, Heather JD. Quantitative measurement of regional cerebral blood flow and oxygen metabolism in man using O-15 and positron emission tomography: theory, procedure, and normal values. *J Comput Assist Tomogr*. 1980;4:727-736.

16. Herscovitch P, Markham J, Raichle ME. Brain blood flow measured with intravenous $H_2{}^{15}O$. I. Theory and error analysis. *J Nucl Med*. 1983;24:782–789.

17. Bacharach SL, Libutti SK, Carrasquillo JA, Measuring tumor blood flow with $H_2{}^{15}O$: practical considerations. *Nucl Med Biol.* 2000;27:671-676.

18. Lodge MA, Carson RE, J.A. Carrasquillo JA, Whatley M, Libutti SK, Bacharach SL, Parametric images of blood flow in oncology PET studies using ^{15}O-water. *J Nucl Med*. 2000;41:1784-1792.

19. Lehtiö K, Eskola O, Viljanen T, et al. Imaging perfusion and hypoxia with PET to predict radiotherapy response in head-and-neck cancer. *Int J Radiat Oncol Biol Phys.* 2004;59:971-982.

20. Logan TF, Jadali F, Egorin MJ, et al. Decreased tumor blood flow as measured by positron emission tomography in cancer patients treated with interleukin-1 and carboplatin on a phase I trial. *Cancer Chemother Pharmacol.* 2002;50:433-444.

21. Green MA, Klippenstein DL, Tennison JR. Copper(II) bis(thiosemicarbazone) complexes as potential tracers for evaluation of cerebral and myocardial blood flow with PET. *J Nucl Med*. 1988;29:1549-1557.

22. Green MA, Mathias CJ, Welch MJ, et al. [^{62}Cu]-labeled pyruvaldehyde *bis*(N^4-methylthiosemicarbazonato)copper(II): synthesis and evaluation as a positron emission tomography tracer for cerebral and myocardial perfusion. *J Nucl Med*. 1990;31:1989-1996.

23. Ng Y, Lacy JL, Fletcher JW, Green MA. Performance of a ^{62}Zn/^{62}Cu microgenerator in kit-based synthesis and delivery of ^{62}Cu–ETS for PET perfusion imaging. *Appl Radiat Isot.* 2014;91:38-43.

24. John E, Green MA. Structure-activity relationships for metal-labeled blood flow tracers: comparison of ketoaldehyde *bis*(thiosemicarbazonato)copper(II) derivatives. *J Med Chem*. 1990;33:1764-1770.

25. Mathias CJ, Welch MJ, Perry DJ, et al. Investigation of copper-PTSM as a PET tracer for tumor blood flow. *Nucl Med Biol.* 1991;18:807-811.

26. Mathias CJ, Green MA, Morrison WB, Knapp DW. Evaluation of Cu-PTSM as a tracer of tumor perfusion: comparison with labeled microspheres in spontaneous canine neoplasms. *Nucl Med Biol.*, 1994;21:83-87.

27. Herrero P, Markham J, Weinheimer CJ, et al. Quantification of regional myocardial perfusion with generator-produced ^{62}Cu-PTSM and positron emission tomography. *Circulation*. 1993;87:173-183.

28. Beanlands RSB, Muzik O, Hutchins GD, Woulfe ER, Schwaiger M. Heterogeneity of regional nitrogen-13-labeled ammonia tracer distribution in the normal human heart: comparison with rubidium-82 and copper-62-labeled PTSM. *J Nucl Cardiol.* 1994;1:225-235.

29. Herrero P, Hartman JJ, Green MA, et al. Assessment of regional myocardial perfusion with generator-produced ^{62}Cu-PTSM and PET in human subjects. *J Nucl Med*. 1996;37:1294-1300.

30. Melon PG, Brihaye C, Degueldre C, et al. Myocardial kinetics of K-38 in humans and comparison with Cu-62-PTSM. *J Nucl Med*. 1994;35:1116-1122.

31. Okazawa H, Yonekura Y, Fujibayashi Y, et al. Clinical application and quantitative evaluation of generator-produced copper-62-PTSM as a brain perfusion tracer for PET. *J Nucl Med*. 1994;35:1910-1915.

32. Wallhaus TR, Lacy J, Stewart R, Bianco J, Green MA, Stone CK. Copper-62-pyruvaldehyde bis(N^4-methylthiosemicarbazone) PET imaging in the detection of coronary artery disease in humans, *J Nucl Cardiol*. 2001;8:67-74.

33. Green MA, Mathias CJ, Willis LR, et al. Assessment of Cu-ETS as a PET radiopharmaceutical for evaluation of regional renal perfusion. *Nucl Med Biol*. 2007;34:247-255.

34. Shelton ME, Green MA, Mathias CJ, Welch MJ, Bergmann SR, Kinetics of copper-PTSM in isolated hearts: a novel tracer for measuring blood flow with positron emission tomography. *J Nucl Med*. 1989;30:1843-1847.

35. Mathias CJ, Welch MJ, Raichle ME, et al. Evaluation of a potential generator-produced PET tracer for cerebral perfusion imaging: single-pass cerebral extraction measurements and imaging with radiolabeled Cu-PTSM. *J Nucl Med*. 1990;31:351-359.

36. Minkel DT, Saryan LA, Petering DH, Structure-function correlations in the reaction of *bis*(thiosemicarbazone) copper(II) complexes with Ehrlich acites tumor cells. *Cancer Res*. 1978;38:124-129.

37. Baerga ID, Maickel RP, Green MA, Subcellular distribution of tissue radiocopper following intravenous administration of ^{67}Cu-labeled Cu-PTSM. *Nucl Med Biol*. 1992;19:697-701.

38. Basken NE, Mathias CJ, Green MA. Elucidation of the human serum albumin (HSA) binding site for the Cu-PTSM and Cu-ATSM radiopharmaceuticals. *J Pharm Sci*. 2009;98:2170-2179.

39. Basken NE, Green MA. Cu(II) bis(thiosemicarbazone) radiopharmaceutical binding to serum albumin: further definition of species-dependence and associated substituent effects. *Nucl Med Biol*. 2009;36:495-504.

40. Mathias CJ, Bergmann SR, Green MA. Development and validation of a solvent extraction technique for determination of Cu-PTSM in blood. *Nucl Med Biol.* 1993;20:343-349.

A.

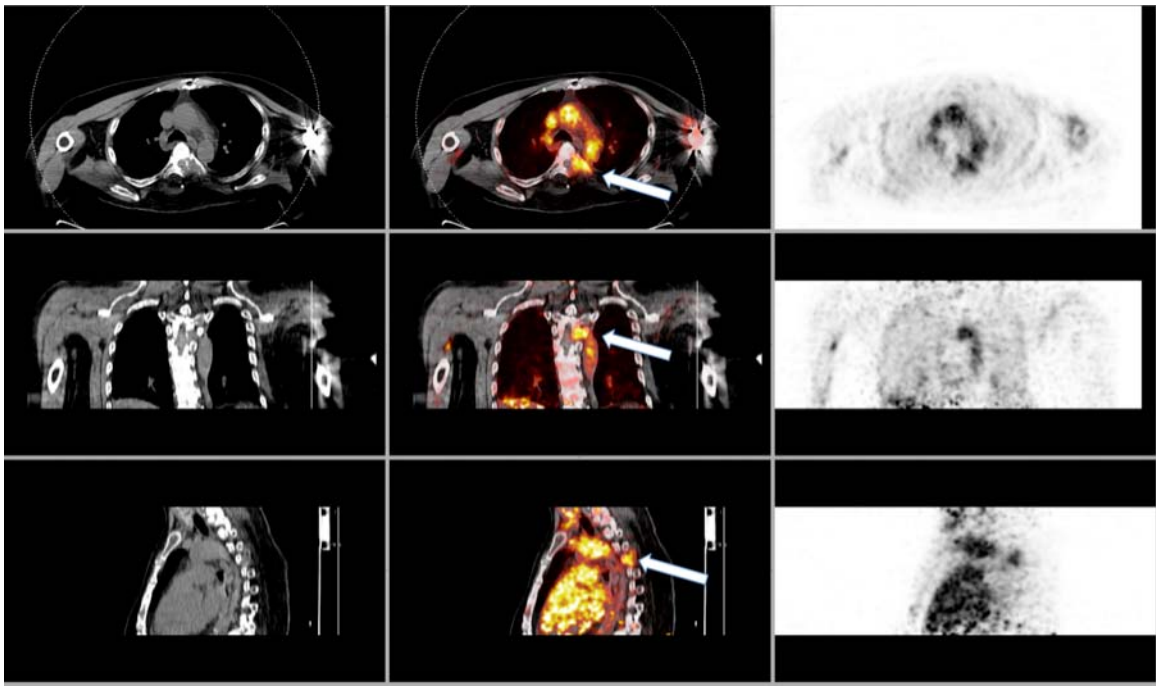

B.

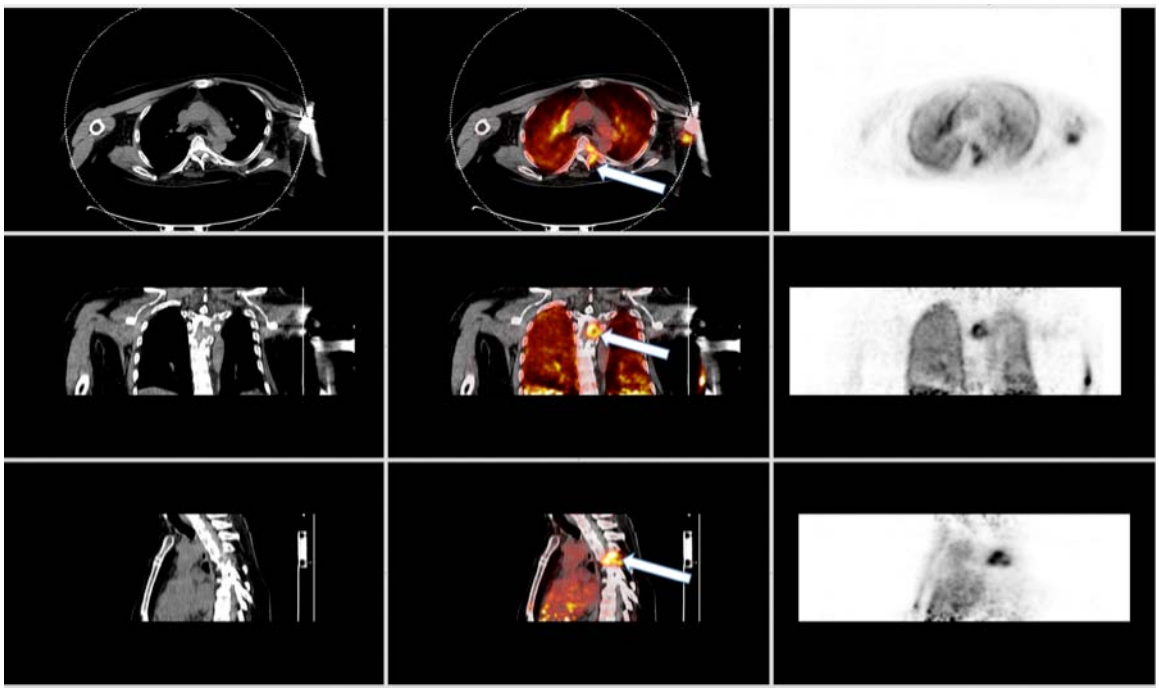

Figure 1. Summed images formed after re-binning the dynamic list-mode data from 0-3 minutes after injection of ^{15}O-water and ^{62}Cu-ETS. In this example and in all other patients, the dynamic, list-mode PET data was obtained in a 21.7 cm z-axis field of view to ensure inclusion of

the cardiac blood pool for determination of the arterial input function used for determination of K_1 for both tracers. **A.** Images from the ^{15}O-water dynamic study, where the CT on left shows a hypodense lesion at T4 that is also seen on fused images (center, white arrow) and PET images (right). **B.** Images from the ^{62}Cu-ETS dynamic study, where again the CT on left shows the hypodense lesion at T4 that is seen on fused images (center, white arrow) and PET images (left). Both the summed ^{15}O-water and ^{62}Cu-ETS demonstrate similar image findings in normal tissues as well as the metastatic T4 vertebral lesion. The elevated perfusion seen in the metastatic bone lesion was typical of all other skeletal lesions.

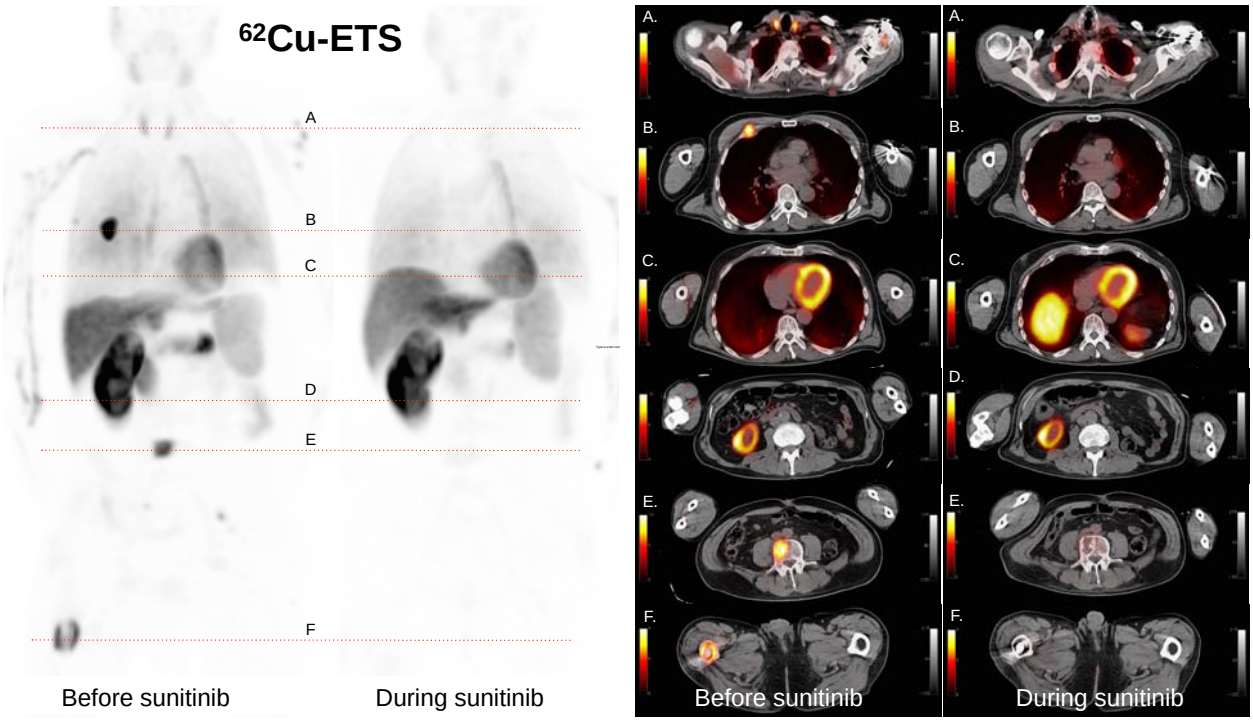

Figure 2. Anterior "whole-body" ^{62}Cu-ETS images are shown on the left, at baseline and during sunitinib therapy, with six corresponding transverse slices of the fused PET and CT images on the right. The six levels correspond to the following structures: Level A – normal thyroid tissue; level B – hyperemic anterior rib lesion on right; level C-normal myocardium and dome of liver; level D – inferior pole of remaining right kidney; level E – hyperemic metastases in L4 lumbar vertebrae; level F – hyperemic metastases in right distal femur. Hyperemic signals in metastatic lesions at baseline are no longer identified on the images obtained during therapy with the anti-angiogenesis agent, while normal tissue signals are similar to baseline. Thyroid tissue signal decreased during therapy, and may relate to previously observed decreases in thyroid function in patients receiving sunitinib. Similar changes were seen in the other subjects.

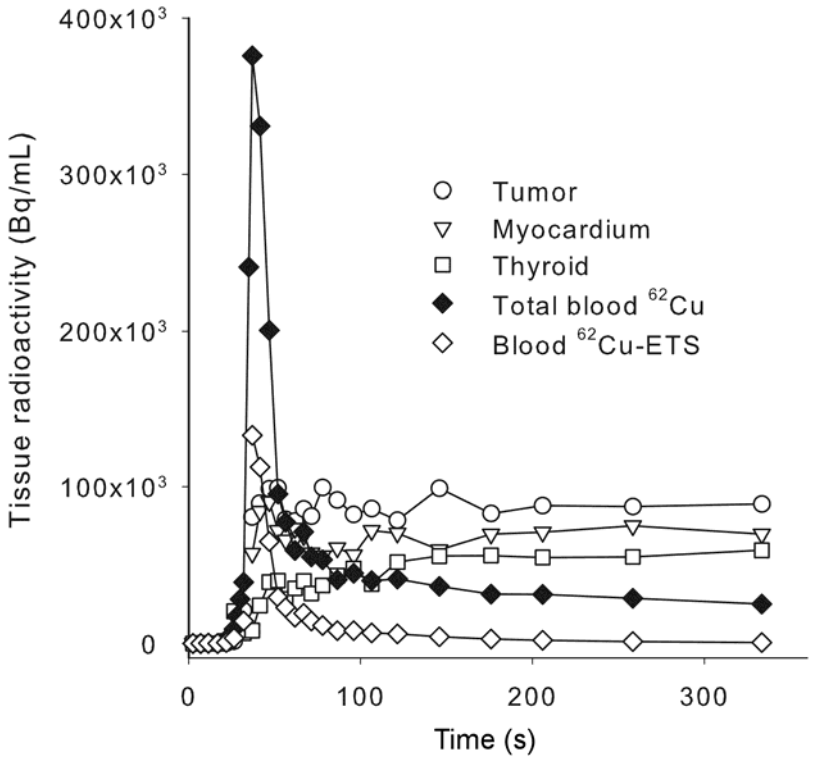

Figure 3. Example of the observed kinetics of blood clearance and tissue uptake following i.v. administration of ^{62}Cu-ETS, derived from the dynamic PET data. The observed left atrial blood ^{62}Cu concentration was corrected to the blood concentration of intact ^{62}Cu-ETS based on the independently measured rate of ^{62}Cu-ETS decomposition by the patient's blood at 37°C *in vitro*.

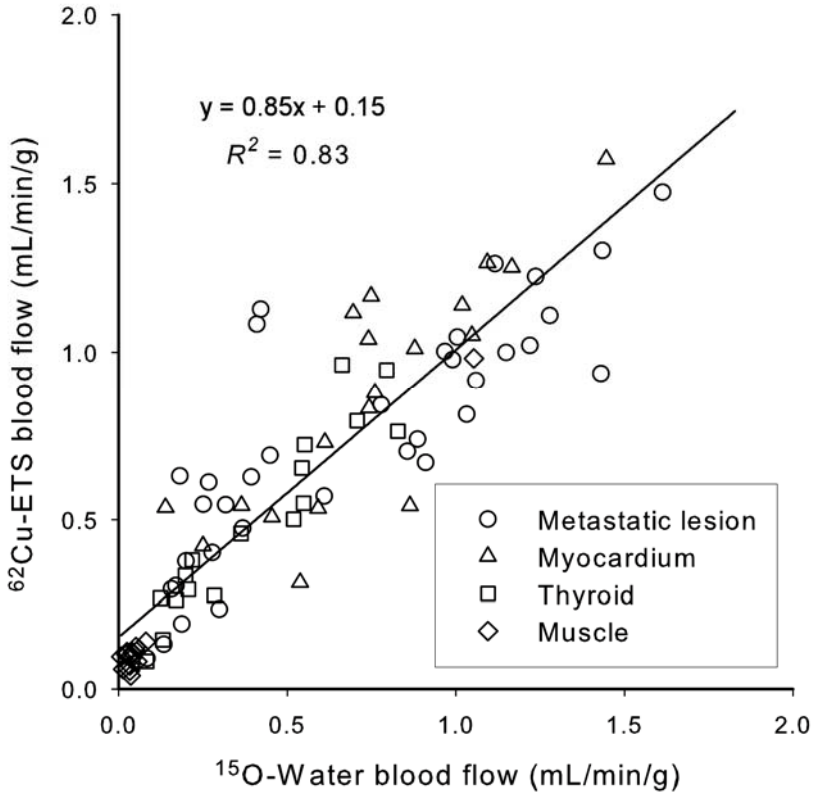

Figure 4. Correlation of the perfusion rate measurements (K_1 values, mL•min^{-1}•g^{-1}) obtained with ^{62}Cu-ETS and ^{15}O-water for normal tissues and metastases (n=88 tissue regions from 18-paired dynamic PET images).

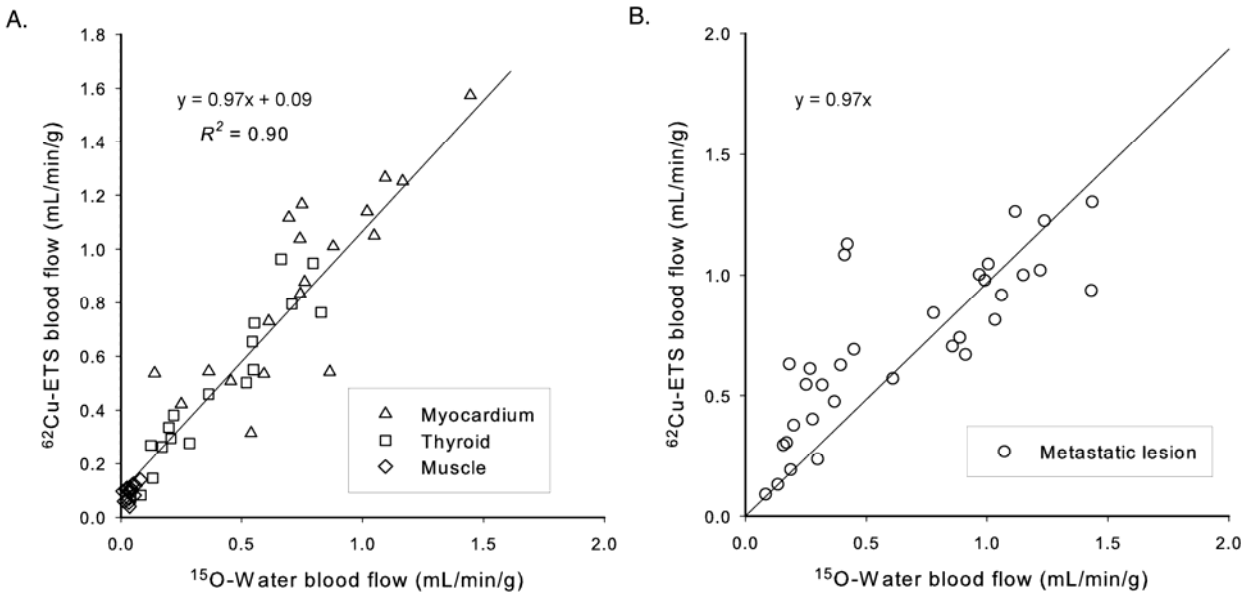

Figure 5. Correlation of the perfusion rate measurements (K_1 values, mL•min^{-1}•g^{-1}) obtained with ^{62}Cu-ETS and ^{15}O-water when the analyses are restricted to tissue regions from normal tissues alone (**A**, n = 53), and metastases alone (**B**, n=35), in the 18-paired dynamic PET studies. For the metastatic lesion data, the regression line shown was forced through the origin, illustrating that a number of the lower flow lesions (all in the lung) are the largest source of variance. The unforced regression line for Figure 5B is: $y = 0.70x + 0.27$; $R^2 = 0.72$.

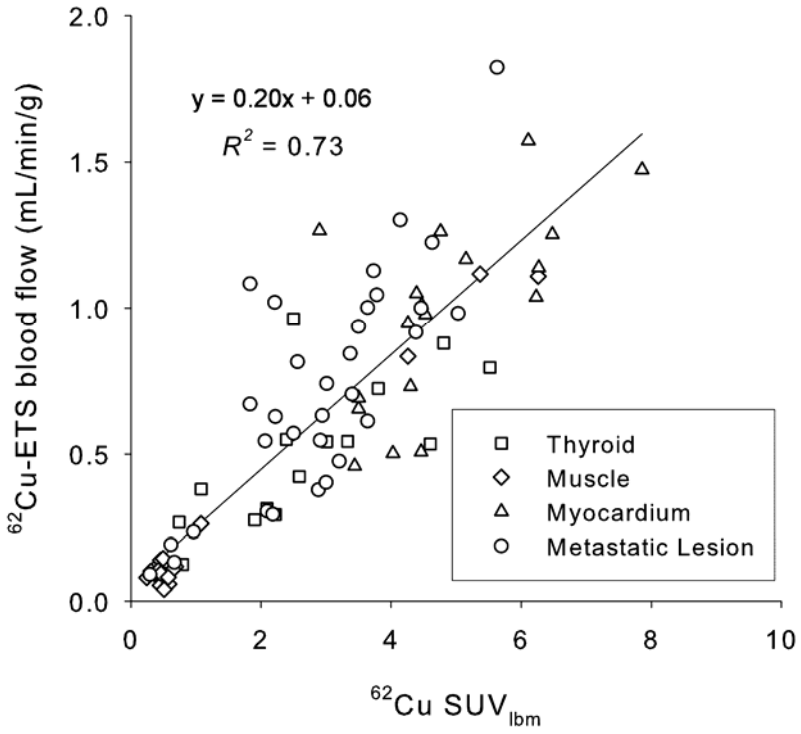

Figure 6. Correlation of mean SUV_{lbm} measurements in the attenuation-corrected whole-body ^{62}Cu-ETS scans with the blood flow values obtained from the preceding dynamic ^{62}Cu-ETS data acquisition.

Table 1: T-Test Statistics for K_1 Values from ^{15}O-water and ^{62}Cu-ETS for Normal Tissues and Metastatic Lesions

^{15}O-K_1 versus ^{62}Cu- K_1	^{15}O- K_1	^{62}Cu- K_1	n	p
All Samples Baseline & Rx	0.55 ± 0.45	0.63 ± 0.42	88	0.28
All Samples - Baseline	0.66 ± 0.49	0.71 ± 0.43	42	0.65
All Samples - Treatment	0.45 ± 0.36	0.55 ± 0.38	46	0.25
Normal Tissues - Baseline & Rx	0.46 ± 0.42	0.54 ± 0.43	53	0.33
Normal Tissues - Baseline	0.53 ± 0.42	0.58 ± 0.42	24	0.66
Normal Tissues - Treatment	0.41 ± 0.42	0.51 ± 0.45	29	0.37
All Lesions - Baseline & Rx	0.69 ± 0.46	0.75 ± 0.38	35	0.56
All Lesions - Baseline	0.84 ± 0.53	0.87 ± 0.40	18	0.81
All Lesions - Treatment	0.53 ± 0.33	0.61 ± 0.32	17	0.47
Muscle-Baseline and Rx	0.05 ± 0.04	0.10 ± 0.05	18	0.00011
Muscle-Baseline	0.05 ± 0.04	0.11 ± 0.02	8	0.0034
Muscle - Treatment	0.05 ± 0.04	0.10 ± 0.06	10	0.072
Thyroid-Baseline and Rx	0.46 ± 0.25	0.54 ± 0.22	17	0.36
Thyroid-Baseline	0.61 ± 0.19	0.69 ± 0.24	8	0.79
Thyroid- Treatment	0.30 ± 0.17	0.41 ± 0.12	9	0.12
Myocardium-Baseline and Rx	0.88 ± 0.35	0.99 ± 0.32	18	0.31
Myocardium-Baseline	0.90 ± 0.32	0.97 ± 0.28	8	0.64
Myocardium - Treatment	0.86 ± 0.39	1.00 ± 0.37	10	0.39

Table 2. Characteristics of the Pulmonary Nodules.

	Initial Tumor Diameter (cm)	Tumor Diameter at Repeat Imaging (cm)	% Change
Mean	2.3 ± 1.4	1.8 ± 1.5	-29%
Range	1.14 - 6.29	0 - 5.04	
Median	1.8	1.6	